Chapter 14

Antispoofing and multispectral (optical) methods in hand-based biometrics

Mona Heidari[1], Tomáš Goldmann[1], Michal Dvořák[1], and Martin Drahanský[1]

14.1 Introduction

Vulnerability of any given security system is an important aspect that needs to be carefully analyzed during design phase. When dealing with biometric systems, one important source of such vulnerability that needs to be especially considered is its tendency to deception by spoofs. Since a high enough quality spoof can become indistinguishable from the original biometric characteristic by human eye, we may need additional methods of spoof recognition. In this chapter, we will investigate several approaches used as an antispoofing method, with emphasis on approaches utilizing the liveness detection (antispoofing).

14.2 Fingerprint recognition

There was no need for a special hardware for acquiring fingerprint images in the past, because fingerprints were kept on dactyloscopic cards using black ink or other dye. These images then could be digitized via a scanner; this method is called off-line sensing [1].

For live-scan sensing, there is no need for the ink; a person just needs to place his/her finger near the electronic fingerprint scanner. The first generation of on-line sensors was based on optical technology [2], but others such as solid-state or ultrasound were invented.

Fingerprints are physiological characteristic, which means that they can be damaged. A user may (un)intentionally harm his finger and make the recognition impossible [3]. There are also security issues. Most users are not observant to the fact that they leave their latent fingerprints on many places such as glasses, doors,

[1]Faculty of Information Technology, Centre of Excellence IT4Innovations, Brno University of Technology, Czech Republic

etc. Such latent fingerprints can be used to create artificial fingertip to fool the sensor and to obtain unauthorized access to a system.

Therefore, there is no wonder that many researchers put a lot of effort in spoofing fingerprint systems and at the same time, developing antispoofing mechanisms.

14.3 Liveness detection on fingers

The capability of a biometric system to detect whether the provided biometric sample is alive or not is denoted as liveness detection [2], and its main purpose is to detect spoofing.

Liveness detection methods can be divided into three categories [1]:

1. Using only data collected for biometric purposes.
2. Using further-processed information collected in order to generate discriminating features or by sensing the biometric sample in time.
3. Using additional hardware.

Liveness detection uses acquired data to determine whether the input biometric characteristic is alive. Properly performed liveness detection should reject all nonbiologic spoofs and majority of the remaining ones, increasing the security of the system during an acquisition stage.

Basic principle of liveness detection and its role in biometric system can be seen in Figure 14.1. The acquisition of liveness data as well as biometric data should ideally be simultaneous and performed on the same part of the biometry in question; otherwise, the attacker can perform separate attack on the individual parts of the system making the task less complex, as the data would only need to meet the liveness requirement at some time/place and be a match to the template at other, creating a possible vector of attack [4]. There are two ways how to

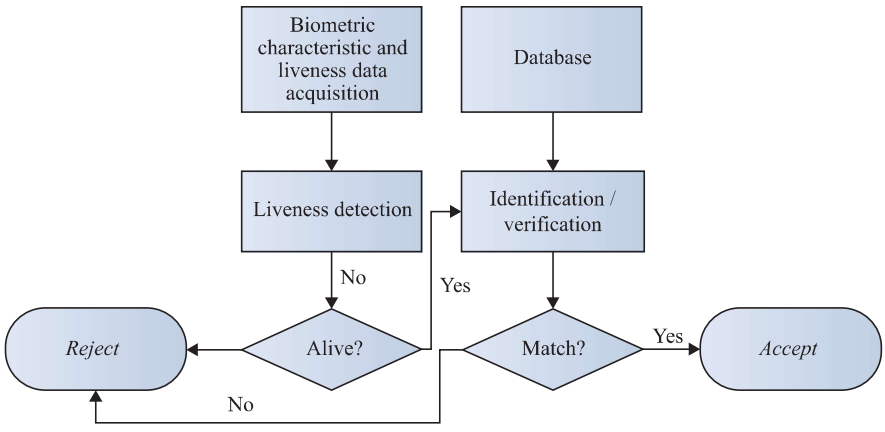

Figure 14.1 Biometric system with liveness detection

determine whether a presented biometric sample is alive or not—liveness detection focuses on unique properties of human body parts and nonliveness detection focuses on typical properties of materials used to fool the system. To discourage potential attackers from presenting a fake finger (i.e., an imitation of the fingertip and the papillary lines) or, even worse, to hurt a person to gain access, the system must be augmented by a liveness detection component [5,6].

Various methods that are used for liveness detection will now be introduced.

14.3.1 Perspiration and sweat pores based detection

One of the several liveness detection methods without any additional hardware is using natural perspiration behavior of skin. Human skin in general, but fingertips especially are covered by sweat glands that excrete sweat fluid. The presence of the pores and of sweat fluid can be used as a mark of a liveness. For the sweat fluid detection, both the optical, chemical and capacitive approach had been explored [7–9]. In Figure 14.2, principle of determining liveness based on perspiration is shown. The spoof incapable of producing sweat fluid would fail to have any change in perspiration measured.

For the pore detection, the systems require, the resolution be high enough to acquire the necessary detail, its viability has been demonstrated as well [8].

14.3.2 Temperature and temperature stimuli based detection

Unlike artificial spoof, which will retain a room temperature without external heat source, human extremities will regulate its own body temperature. The temperature of extremities depends on outside conditions, biological state and stimuli; this temperature will vary in between approximately 25 and 37 °C and can be measured using thermal camera, for example, as can be seen in Figure 14.3.

By measuring this temperature, we can, to an extent, claim that the object in detector is part of human body. However, this method may be compromised, if the hand is undercooled or the room temperature is similar to body temperature. It is also viable to add an active heating element to the spoof, thus bypassing this security feature.

To increase the reliability of this method, we may use additional stimuli. The human skin will react to a stimulus by changing the blood flow to regulate the

Figure 14.2 Temporal perspiration pattern extracted from capacitive sensor [9]

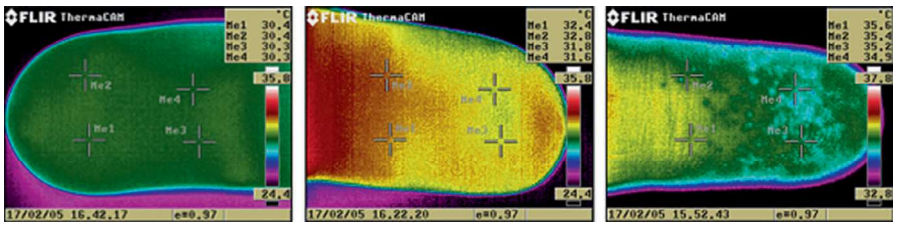

Figure 14.3 Thermographs of human hand showing temperature variation in human finger [10]

temperature. By detecting this change and determining the appropriateness of this change, we may determine the likeliness that observed reaction is that of a human tissue. The downside of this approach is a reaction time. As the stimuli cannot be dangerous, or cause of discomfort, which might compromise the measurement by voluntary or involuntary movement of the subject, the time for change to be observable will be in order of seconds.

14.3.3 Pulse and blood oxygenation based detection

Longitudinal blood pressure wave generated during systolic phase of cardiac cycle, also known as pulse, changes the volume of the blood vessels that can be observed even on the surface of the skin. Observation can be performed by measuring the periodic change in position of human skin [7], or by the minute change in color that occurs due to periodic increases and decreases in the oxygen level of blood.

14.3.4 Multimodal approach

Using additional biometric modalities increases the difficulty to attack the biometric system at the sensor-level [11]. It is more demanding for the attacker, because it needs to elicit additional biometric data from the valid user and create an additional artificial sample, which must be accepted by the attacked biometric system.

14.3.5 Material identification based detection

Human skin, like any material, may undergo various measurements of physical properties due to its nature; these properties may be different from materials used to create a spoof. Electrical properties can be measured, such as resistivity or conductivity, which varies from other materials due to perspiration and salt content in sweat fluid. Reflection of ultrasound presents other source of material analysis, as the ultrasound will penetrate the topmost parts of skin and is then scattered at different frequency, this change can then be measured.

Another approach is to measure the optical characteristics of human skin. This will be investigated in upcoming parts of the chapter.

14.4 Finger vein recognition

There are several ways [11] how to acquire an image of human blood vessels, such as using X-ray, magnetic resonance imaging, ultrasound, far-infrared light, near-infrared (NIR) light or thermal approach [12]. The NIR light approach is used most often in biometrics due its trade-off between cost, power supplement requirements, size of the sensor and quality of resulting image.

The two types of hemoglobin (Hb, HbO_2) have different absorption spectra. Experiments have proved that the permeability of human tissue is high for electromagnetic radiation in the range from 600 to 1,300 nm [11,13]; this range is often called optical window. Especially in the range between 750 and 950 nm [11], the radiation can penetrate deep enough into the skin to reach the superficial arteries and veins, and as a consequence it is absorbed in blood vessels, due to higher absorption coefficient blood. This effect can be captured by a camera on the image that shows where blood vessels are located, are darker. Even though the described method can not only capture veins, but also arteries, this method for capturing blood vessels will be further denoted as a vein characteristic.

There are two main methods of acquiring an image of blood vessels of a finger with NIR approach-reflection and transmission.

14.4.1 Reflection method

The finger is illuminated by NIR light, and the partially reflected radiation is captured by a CCD camera, which is located on the same side of the finger as the light emitter. Because veins are closer to the skin than arteries, veins are usually captured on a resulting image. Simplified schema of a finger vein sensor using reflection method can be seen in Figure 14.4(a).

The main advantages of this approach are the sensor size, compactness and possibility to easily extend existing (fingerprint) systems with finger vein recognition system.

14.4.2 Transmission method

The transmission method is usually used only in finger vein recognition, because fingers are generally thin enough to allow the light to pass through the tissue. The NIR light emitter is in such case located on the opposite side of the finger than the camera. Although the transmission method is leading in finger vein sensing, it must be mentioned that the device itself is usually larger than the one using reflection method. On the other hand, the quality of resulting image is more high-contrasted in comparison to reflection approach [14]. Simplified schema of a finger vein sensor using reflection method can be seen in Figure 14.4(b).

14.4.3 Wavelength of light emitters

The range, where the permeability of human tissue is high, is very wide from 600 to 1,300 nm [11]. The absorbency of hemoglobin also differs. Until today, it has not been proven, which wavelength is generally the best suitable for transmission and

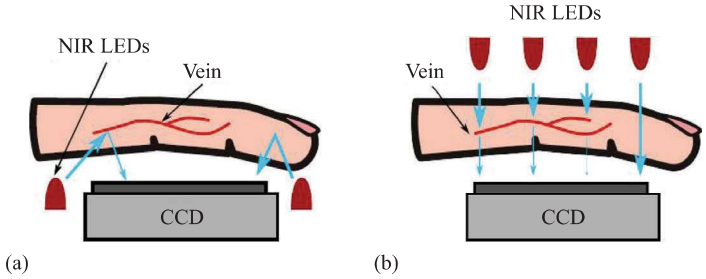

Figure 14.4 Two main approaches for acquiring finger vein pattern using NIR light: (a) refection method and (b) transmission method

reflection method. Yang and Shi [15] describe a finger vein sensor using 760 nm LEDs with declaration that this is the optimal light source wavelength to capture veins.

14.5 Spectral analysis approach to spoof detection

Hand-based biometric systems may have antispoofing methods based on several approaches. One of the approaches is liveness detection, which can be realized with parts of hand. Although it is possible to perform lifetime detection based on skin temperature, electrical resistance, electrical conductivity or bio-impedance, these methods are not reliable [16]. However, there are more reliable methods to help determine if spoofing has occurred.

Like other parts of the human body, heartbeat can be detected in the hand. When heart pumps oxygenated blood to veins, there are volume changes in the veins and vessels. Therefore, the pulse can be detected on the skin of finger. With a very accurate laser rangefinder, these changes can be recorded to determine whether spoofing has taken place or not.

Another aspect that affects the skin's properties is the actual blood flow, which can vary depending on many factors, e.g., body temperature. By analyzing the image obtained by illuminating the skin of different wavelengths, it is possible to get a picture of the different parts beneath the surface of the skin and verify that it is really human skin. It is possible to use several light sources of different wavelengths for a single exposure [17]. This is the basis for multispectral analysis of the human skin. The main advantage is the ability to use multispectral analysis based on image data to assess the health condition epidermal layer of the skin or detect spoofing.

With biometric system using a multispectral analysis, it is very difficult to perform a spoofing attack because homogeneous materials cannot be used.

Human skin is a multilayered organ. Every layer, fulfilling different functions, has different properties; these differences can become evident during optical analysis. There are two major methods to this approach. Either the light directly

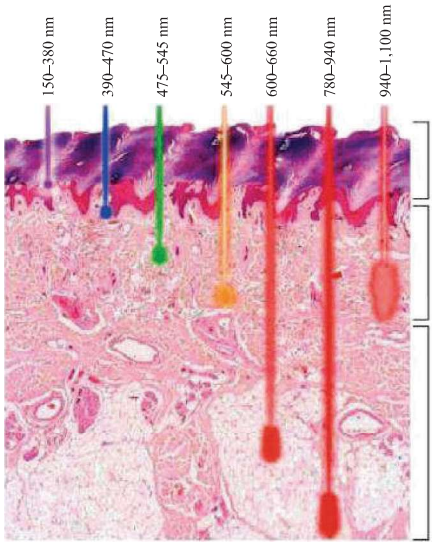

Wavelength (nm)	Color	Penetration (mm)
150–380	Ultraviolet	<0.1
390–470	Violet - cobalt blue	~ 0.3
475–545	Blue - green	~ 0.3–0.5
545–600	Yellow - orange	~ 0.5–1.0
600–650	Red	~ 1.0–2.0
650–950	Carmine red - infrared	2–3
950–1,200	Infrared	1

Figure 14.5 Depth of skin penetration based on wavelength [18]

reflected from the skin is analyzed, or the system analyzes the dispersed light generated after its propagation through the skin.

14.5.1 Using the dispersed light

Due to different composition of different layers of the skin, various wavelengths will experience different absorption rate at different layers. In Figure 14.5, we can see an example of such differences. The image outlines the average penetration distance into the skin based on the wavelength of a chosen light.

Based on these properties, an innovative approach to liveness detection can be proposed. This system will use the variation in absorption as a function of wavelength. For the system to work, a source of light is required and photosensitive parts that will record the rate and characteristics of absorption.

In Figure 14.6, the prototype developed for verifying the hypothesis is presented. It supports placement of light-emitting diodes of various wavelengths, wide spectrum photodiodes for overall absorption rate information and RGBW (Red Green Blue White) detectors, to analyze the absorption at individual color channels [17].

The range of wavelengths has been investigated, such as infrared LEDs of wavelengths 740 and 940 nm, ultraviolet LED with wavelength of 400 nm and RGB LED with dominant wavelengths of 650, 520 and 460 nm.

Via experimentation, it has been determined that measuring the characteristics of dispersion from RGB LED and 740 nm IR LED is a viable method of liveness detection. At these wavelength ranges, the characteristics were distinguishable from the most common materials used for spoof construction.

To attack this antispoof method, a nonhomogeneous, multilayer spoof would need to be developed, and to the knowledge of the authors, no research has been

Figure 14.6 Liveness detector—prototype

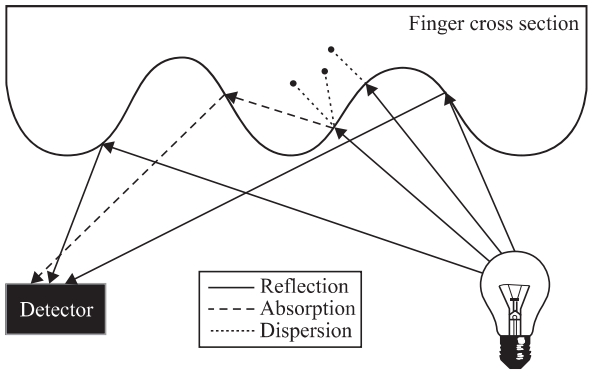

Figure 14.7 Liveness detection based on spectral characteristics [20]

performed in this area of hand spoof development. The UV light presented mixed results, the spectral characteristics of dispersed light was differentiable from most spoofs, but the interclass variability was too large, influenced by a skin pigmentation. Further research needs to be performed in this area.

This method however presents a disadvantage, as the analyzed hand needs to be in contact with the device, to eliminate the effect of reflected light. By forming a seal around the chosen LED, the only source of light that reaches the sensors is the light that propagates through the skin and tissue. This prevents the construction of the touchless biometric system using this technology. To overcome this limitation, another approach to spectral analysis needs to be used. Viable alternative comes in the form of analysis of reflected light.

14.5.2 Using reflected light

In Figure 14.7, the difference between reflection and dispersion is outlined. Whereas the dispersion utilizes only the light that has penetrated the skin, the sensors based on reflection use the directly reflected light and dispersed. The observed characteristics of various wavelengths reaching the detector are then used for the liveness detection [19]. Using this principle, the biometric sensor may be touchless.

To determine liveness based on reflected light properties, an appropriate wavelength must be chosen. To enable this system more for integration into current technologies, the wavelengths in ranges used by current cameras used in a biometric sensor are preferred; for that reason, wavelengths of 400, 410, 470, 525, 550, 570, 590, 635, 700 and 800 nm have been investigated. In Figures 14.8 and 14.9, we can see a finger illuminated using some of these wavelengths.

Liveness detection can be then performed in the following steps:

- During acquisition, a skin sample is sequentially illuminated using chosen wavelengths and the images are being acquired
- The image is blurred to eliminate glares and unwanted artifacts
- Pixels/pixel ranges are extracted in a repeatable manner as features
- Feature vector is constructed
- Classification is performed

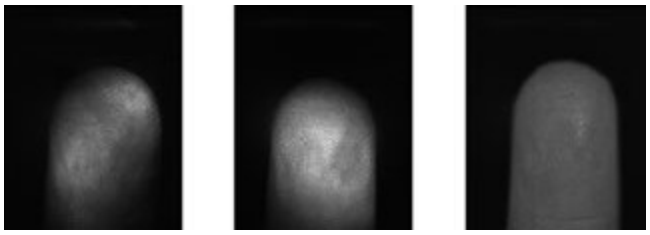

Figure 14.8 Fingertip illuminated using LED of 400 (left), 470 (middle) and 525 nm (right)

Figure 14.9 Fingertip illuminated using LED of 550 (left), 635 (middle) and 700 nm (right)

Figure 14.10 Fingerprint acquisition device [21] (left) and hardware modification for liveness detection (right)

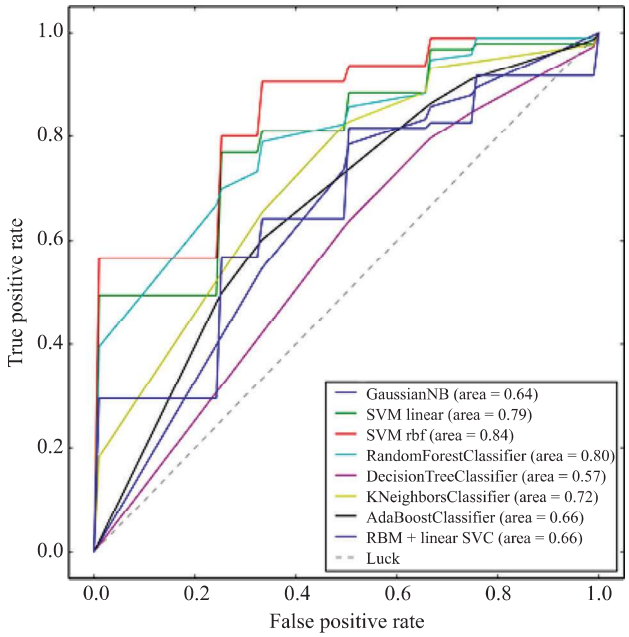

Figure 14.11 ROC of liveness detection based on optical properties using various machine-learning algorithms

As was indicated, the advantage of this approach lies in ease of integration into existing systems. Any optical based biometric system only needs to integrate the light source of chosen wavelengths into itself. As we can see in Figure 14.10, existing biometrics solution can be simply modified to support this method of liveness detection.

Due to feature vector being constructed from potentially large amount of data, an appropriate machine-learning method needs to be utilized to prepare a strong classifier.

Figure 14.11 shows performance of classifiers, constructed using various machine-learning approaches, with strongest being created using the support vector machine with radial basis function kernel.

From the figure we can also see that the underlying principle is valid, but further research needs to be performed to perfect this approach.

14.6 Hematoma (improvement of antispoofing methods in the presence of hematoma)

Hematoma, popularly called bluish or bruise, is caused by bleeding from damaged blood vessels under the skin. The word comes from the Greek words *hema* and *soma*, which means blood and body. There are many cases of hematoma; the hematoma is primarily due to trauma. It is caused by a strong pressure and/or a stroke that causes damage to the bloodstream. After it, the blood leaks from vessels and veins to interstitial space. The human organism has mechanism to stop blood leakage and is based on vessels contraction and hemostatic substances. As a result of these circulatory system mechanisms, the human organism can protect itself against a large loss of blood. In this case, hematoma almost disappears from organism after some time. In some cases, the large hematomas need to be removed surgically.

The other cause of the formation hematoma is fragile meningococcal meningitis, autoimmune diseases such as congenital and acquired disorders blood clotting, absence of vitamin K, liver disease, bone marrow disorders and low blood platelet counts, e.g., thrombocytosis [22]. The hematoma is a common problem encountered by every human. In the field of medicine, hematoma is named by localization on the human body. Accordingly, examples of some hematomas:

- *Subdermal hematoma* is hematoma located below skin (commonly called bruise)
- *Subgaleal hematoma* is boundary accumulation of blood between Epicranial aponeurosis and periosteum [23]
- *Cephalohematoma* is boundary accumulation of blood under the periosteum that covers most of the cranial bone in hairy head [23]
- *Epidural hematoma* is local accumulation of blood between cranial bones and dura mater [24]
- *Subdural hematoma* is hematoma beneath the dura of skull or in the spinal cord [24]
- *Subarachnoid hemorrhage* is extravasation of blood into the subarachnoid space [24]
- *Auricular hematoma* is boundary accumulation of blood located between skin and cartilage of ear [25]

- *Monocular hematoma* occurs when soft tissue is injured or the bones of face are fractured [26], while the binocular hematoma occurs around the fractured bones
- *Perianal hematoma* is acute thrombosis of the anal blood vessels
- *Intermuscular hematoma* occurs between muscles
- *Intramuscular hematoma* occurs into muscle
- *Subungual hematoma* occurs under nail [27]

Of these types of hematomas, the subdermal hematoma can be used as part of antispoofing solution. The subungual hematoma is visible too, but multispectral properties are affected by nail, which overlaps the hematoma. For capturing, multispectral properties are using the devices described in the previous section.

14.7 Hematoma stages

The human body contains a lot of chemical substances; in the case of blood, it is the same too. After a hematoma formation, chemical reactions between the blood components and other chemicals of the human organism begin. Therefore, the properties of hematoma change over time. Time evolution of the hematoma can be divided into five stages according to the hemoglobin conversion. From a multispectral point of view, hemoglobin is an important chemical substance that has a significant influence on light absorption. The color of hemoglobin depends on iron atoms and oxygen [28]. The following stages are divided by hemoglobin conversion to other chemical substances [29]. For us, however, it is important that bruise color is different in each stage [30].

In the biometrics field, multispectral scanning can be used for extraction distribution on veins and vessels. Since the different types of hemoglobin have different absorption coefficient, veins and vessels image can be extracted separately. Since the distribution of veins exhibits a high degree of variability, this can be used as biometrics. The vein authentication device convert image with vessel lines into binary image and then compare with template from the database.

14.7.1 Stage—oxyhemoglobin

After the trauma, the red blood cells (RBCs) are extravasated from the bloodstream into the interstitial space. If trauma causes subdermal hematoma (bruise), a red or blue spot appears on the skin. In the stage, the extravasated hemoglobin (oxyHb) in RBCs can still carry oxygen; therefore, the spot has color depending on the ratio of oxygenated and deoxygenated hemoglobin (deoxyHb). The edges and area of bruise look according to location and how much the blood vessels have been damaged [31]. The oxyhemoglobin has at the beginning of the NIR spectrum (around 700 nm) a lower rate of absorption coefficient than deoxyhemoglobin, shown in Figure 14.12. In the stage, it can be determined whether this is a venous or vascular bleeding by NIR light and photo sensor.

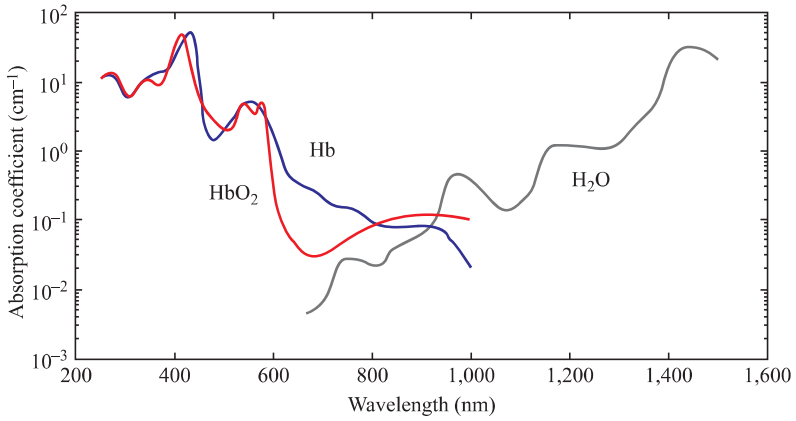

Figure 14.12 Absorption spectra of hemoglobin—Hb, deoxyhemoglobin; HbO_2, oxyhemoglobin; H_2O, water [2]

14.7.2 Stage—deoxyhemoglobin

After 1–5 days, almost all molecules of hemoglobin do not contain oxygen. According to one plausible theory, when the oxygen is not bound in hemoglobin, the color is less red than then color of oxyhemoglobin, and therefore the hemoglobin absorbs redder spectrum [32]. If the red wavelengths are subtracted, the blue spectrum is more predominate; therefore, skin has bluish color [33]. This phenomenon is called cyanosis. Therefore, the color of bruise gradually turns shades of blue. According to previous information, deoxyhemoglobin has different spectral properties against the oxyhemoglobin.

For hematoma detection, the stage provides best conditions, because color difference between area without and with hematoma is the biggest of all stages, as shown in Figure 14.13.

14.7.3 Stage—biliverdin

The hemoglobin breakdown process begins 5 days later. First, the molecule of deoxyhemoglobin is divided into molecules of globin and molecules of heme. Then the molecules of heme are split by enzyme on hemoxygenase and molecule of oxygen into tetrapyrrole, which is called biliverdin. During the process, the equimolar amount of ferro cation (Fe^{3+}) is relaxed too [34]. Because the biliverdin contains conjugated double bond, the biliverdin has a green color.

14.7.4 Stage—bilirubin

After 7 days, the bruise changes color from shades of green to shades of yellow. This is caused by conversion of biliverdin to bilirubin. Conversion from biliverdin

Figure 14.13 Hematoma in the second stage

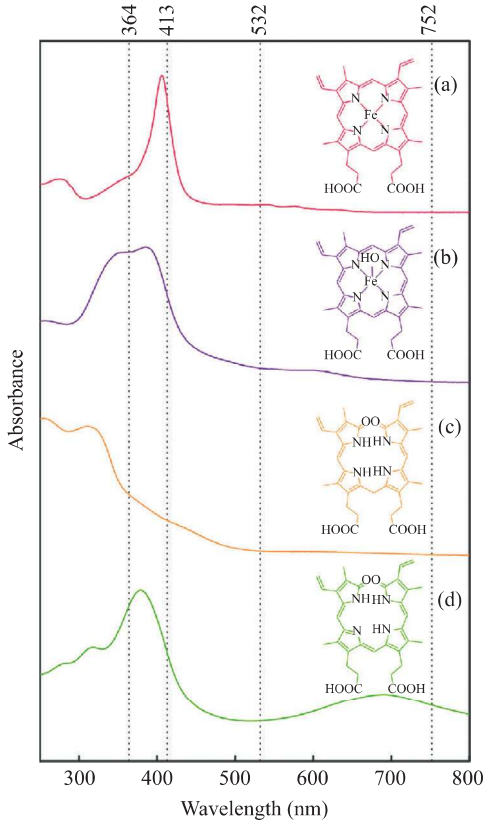

Figure 14.14 Schematic chemical structures and absorption spectra in aqueous solution of the heme chromophores: a—hemoglobin (red), b—hematin (purple), c—bilirubin (orange), d—biliverdin (green)

is carried out using a coenzyme nicotinamide adenine dinucleotide phosphate that occurs as part of the metabolism of organisms. Because bilirubin is the main product of heme degradation, it participates most in the resulting color of the hematoma at this stage [34,35]. According to Figure 14.14, the bilirubin has different spectral characteristics than biliverdin, the greatest difference being in the range from 300 to 364 nm wavelength.

14.7.5 Stage—hemosiderin

After that, all the RBCs may be resorbed, and the skin resumes its normal color. In some cases, ferro cation (Fe^{3+}), which is product of heme catabolism, is taken up by macrophages and degraded into hemosiderin [36]. This causes the coloring of bruise from yellow to brown. The main disadvantage of hemosiderin is that it can cause pigment stains which can last a long time.

However, the stages of hemoglobin conversion may seem unimportant in terms of antispoofing, the opposite is true. The stages of hematoma can be useful information for liveness detection, since spectral properties of hemoglobin and hemoglobin products are quite unique. When hematoma is detected on the hand, we can use multispectral analysis for precision liveness detection. For this reason, hematoma localization is important for the possibility of further evaluation.

14.8 Hematoma detection

The success of hematoma detection depends on the shape, shade of hematoma color and skin color. In the stages 1–4, hematoma has more intense color than normal skin of europoid (light skin). However, when the human has dark skin, it can be assumed that the detection based on skin color will be inaccurate. The process of hematoma detection on light skin can be divided into five stages, shown in Figure 14.15.

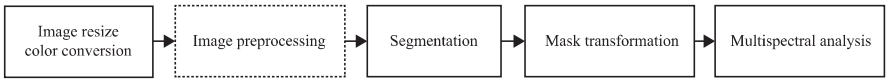

Figure 14.15 Hematoma detection process

14.9 Image resize and color conversion

For faster hematoma segmentation, it is advisable to downscale the size of the input image. If the image has low resolution, this step can be skipped. Most algorithms for hematoma detection are faster with the downscale image than with original image. In the last step, all coordinates of edges of hematoma must recalculate with scale coefficient. The coefficient is determined from the aspect ratio of the original

and the reduced image. Almost all images are saved in the RGB color representation; but for some algorithms, it is better to use Hue Saturation Value (HSV) representation [37]. Therefore, color conversion is the useful step for next image processing. Saturation between areas is useful information for hematoma segmentation.

14.9.1 Image preprocessing

During image processing, it is often needed to remove high-frequency areas from the image. In the other words, the noise needs to be reduced. One way to remove noise is to use the convolution mask that represents selected function, e.g., Gaussian function.

14.9.2 Segmentation

After editing the image, the objective is to get a binary image consisting of two areas. One area is made up of an object of interest (hematoma), and the other consists of a background. This part of algorithm is the most important, but also it is the most difficult to implement. The simplest method is thresholding based on the difference in brightness. However, the method has bad performance when the skin color is dark. Advanced methods can be based on texture analysis and thresholding multiple color channels.

In some cases, the binary area, which represents area without hematoma, contains small enclosed areas. Areas that do not belong to the hematoma are scattered across the area, so it is advisable to remove them using a morphological operation [38]. These disadvantages can be removed by morphological operation *Open*. After the operation is used, the binary mask has smooth and straight contours, and background mask does not contain noise.

14.9.3 Scale and border extraction

If edges of hematoma for advanced algorithms are needed, they should be extracted from binary mask. The morphological operation erode is using for creation edges of hematoma. The resulting contour is obtained by subtracting the mask after applying the erosion filter from the input binary mask, as shown in Figure 14.16. If the input image was downscaled, the mask must be upscaled by the ratio from the first step. The output mask defined localization of hematoma and can be used for accuracy liveness detection.

Figure 14.16 Outline extraction

14.10 Multispectral analysis

After localization, the hematoma is analyzed. The easiest solution is creating histogram for all hematoma stages and comparing them. This approach is strongly affected by various hematomas; therefore, it is not as good as antispoofing solution. Enhancements should be achieved using histogram-based feature vectors from different color representations, such as RGB + HSV. A better method can be based on spectral analysis. According to previous information, the hematoma (bruise) has different absorbance across an electromagnetic spectrum in individual phases. This feature can be used to determine whether it is a fake hand or none. Histogram-based algorithms may not detect fake based on artificially created color spot; therefore, the multispectral approaches are better. Among the problems of this detection are the effects of other chemical substances on the body and probably the possibility to use a hand several hours after death. After death, however, hemoglobin degrades to other substances, but conversion from oxyhemoglobin to deoxyhemoglobin is the same from living to dead tissue. Unfortunately, the bruises are affected by other chemical substances and physical phenomena. For example, about 20 hours after death, the pH of blood decreases to 5.5, which affects other chemical processes in the decomposition of the body [39]. Real use of the postmortem hand for spoofing will have to be verified by other experiments.

Despite everything, the multispectral analysis of hematoma to improve the accuracy of antispoofing methods is an unconventional but interesting approach. However, multispectral skin analysis has a great benefit for liveness detection.

14.11 Liveness detection system based on finger vein pattern

The liveness detection can be perceived from a different point of view. The main task is to distinguish presented biometric samples between living and nonliving classes. The requirements on the proposed system are as follows:

- The system is divided into two separated subsystems acquisition of images and image processing.
- The first subsystem is built using existing fingerprint sensor.
- The second subsystem must be hardware independent, and fully automated input image is automatically classified as live or nonlive without any user input.
- The second subsystem supports a "recognition" mode, which, instead of classification into live or nonlive category, verifies registered users.

14.11.1 Image acquisition

First step in liveness detection on fingers is the acquisition of a presented finger. For our experiments in the laboratory, we selected a TBS fingerprint sensor and extended it with liveness detection based on finger vein pattern (Figure 14.17), however this solution is suitable for any touchless fingerprint reader.

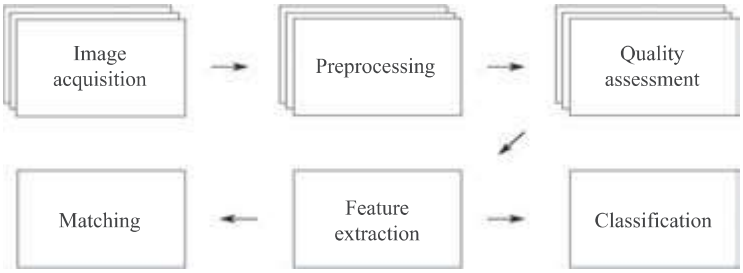

Figure 14.17 Designed architecture of a proposed system

14.11.2 Touchless biometric systems fingerprint sensor

Commercial device TBS 3D-Enroll is a three-dimensional touchless sensor for enrollment and generation of fingerprint templates. There are three cameras inside the sensor as can be seen in Figure 14.10 and several LEDs of various colors. It should be mentioned that the sensor is designed to acquire only a fingertip and therefore a user inserts only this part of the finger into the box. The sizes of both veins and arteries decrease with the distance from heart. For vein recognition, usually the most interesting are parts of finger areas near the middle and proximal phalanges. The blood vessels near distal phalanx are hardly visible, but only image of this finger part is acquirable using this device.

14.11.3 Extension of an existing sensor

Two different methods of sensing are reflection and transmission.

The main disadvantages of transmission method are the size of the device and that a user must put his finger into a "black box." On the other hand, it seems that the transmission method gives images, where the finger veins are more visible and easily distinguishable in comparison to reflection method. Since all these disadvantages are already present in a TBS sensor, the transmission method was chosen to obtain a more high-contrast images. A decision to utilize only the middle camera for this prototype was made; but in future, all three cameras could be used to reconstruct the 3D model of blood vessels of the finger. A board was constructed that five NIR LEDs could be mounted to the top of the fingerprint sensor and the construction allowed effective changing of LEDs and the voltage. The board is powered from the sensor's main power supply, so no additional power supply is needed.

LEDs are connected in parallel to allow one to set different levels of intensity for each LED, because the fingertip thickness and tissue characteristic varies for everyone.

Many finger vein solutions [14,40,41] use automatic brightness control to eliminate such individual variations; thus, the system can be extended with this automated approach. This solution was not incorporated in this work, because it increases both hardware and software demands. After several experiments, we decided to give the resistor R_1 higher resistance in comparison to others ($R_2 = R_3 = R_4 = R_5$) (Figure 14.18).

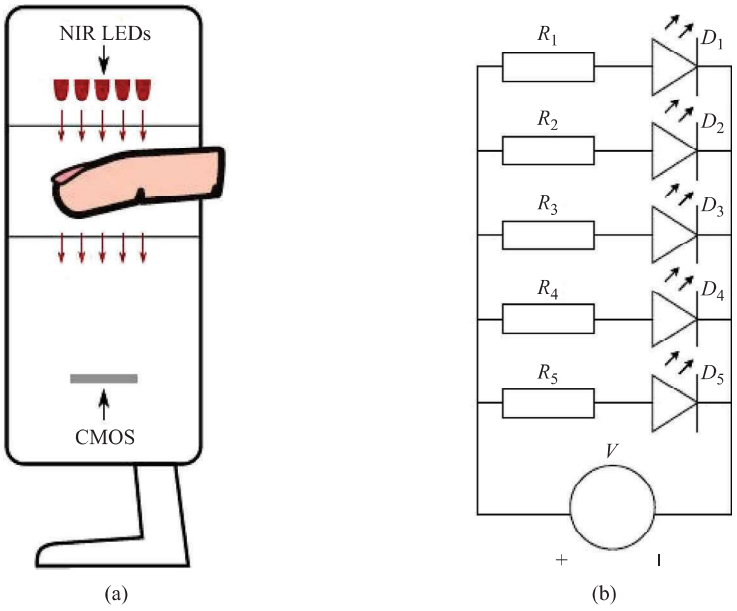

Figure 14.18 Proposed solution of finger vein sensing: (a) overall view and (b) wiring diagram of the extension circuit

The various thicknesses of a finger make it difficult for choosing a general camera setting. As can be seen in Figure 14.19, when a thin (top row) finger is captured, a shorter exposure time is needed in comparison to thicker ones (bottom row). A possible software solution combines images of the finger with different exposure times using high dynamic range imaging (HDR) technique, which produces a single-HDR image with greater dynamic range of luminosity. A different solution is to capture several images with various exposure times and then to use quality evaluation algorithms to choose the best from image series. Since the camera had to be reprogramed each time, the exposure time is changed to capture a sequence of images taking several seconds, and therefore HDR approach could not be utilized due to possible finger posture changes.

14.12 Preprocessing

For the preprocessing of the originally captured images, first, the image is segmented to obtain the finger mask, and after that the elimination of finger posture changes will be described.

14.12.1 Region of interest localization

Conventional algorithms for finger vein region of interest (ROI) localization assume touch-based sensor, and therefore, the ROI of the finger is obtained by applying a fixed window mask. This straightforward approach cannot be used in

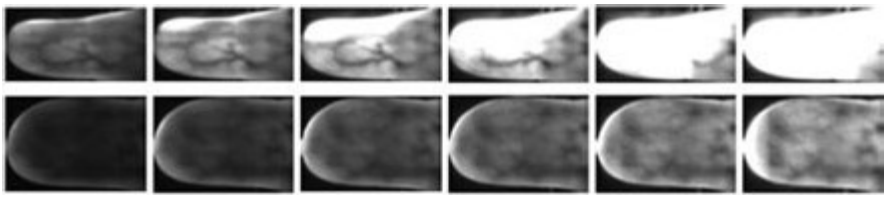

Figure 14.19 *Finger vein images captured with different exposure times. In each row, there are images of the same finger, and appropriate columns belong to the same exposure time. The exposure time grows in the right. All images were enhanced using CLAHE*

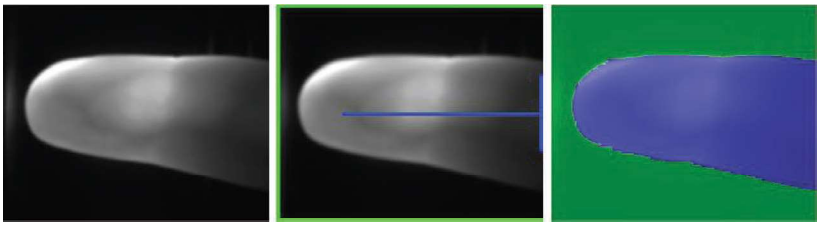

(a) (b) (c)

Figure 14.20 *Example of Watershed procedure. needle blue of part (b) W_f, background green of part (c) W_b. (a) Original image, (b) defined marker sets and (c) segmented image*

most touchless systems, and therefore a method using Watershed for ROI localization will be introduced.

The Watershed algorithm was utilized to distinguish between the finger and the background.

To use the Watershed algorithm, for all classes, there must be preset a set of pixels, which belong to the appropriate class. Let us denote the image size as a tuple (x_m, y_m). The background marker set W_b is defined using (14.1), and the finger marker set W_f using (14.2). Examples of predefined sets can be seen in Figure 14.20(b), and the result of the Watershed algorithm is displayed in Figure 14.20(c).

$$W_b = \{(1,y)|y \in \{1,\ldots,y_m\}\} \cup \{(x,y)|x \in \{1,\ldots,x_m\} \wedge y \in \{1,y_m\}\} \tag{14.1}$$

$$W_f = \left\{(x,y)\middle|x \in \left\{\frac{1}{4}x_m,\ldots,x_m\right\}, y = \frac{1}{2}y_m\right\} \cup \left\{(x_m,y)\middle|y \in \left\{\frac{1}{3}y_m,\frac{2}{3}y_m\right\}\right\} \tag{14.2}$$

According to the segmented image, mask $M(x, y)$ is defined, it returns 1 if (x, y) belongs to the finger segment, 0 otherwise. To reduce possible inaccuracies in segmentation, the morphological opening is applied on finger mask M, followed by morphological closing.

Table 14.1 Defined coordinate system and six finger posture changes based on [42]

Type	Name	
1	Shift along *x*-axis	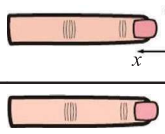
2	Rotation around *x*-axis	
3	Shift along *y*-axis	
4	Rotation around *y*-axis	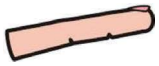
5	Shift along *z*-axis	
6	Rotation around *z*-axis	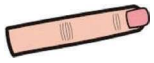

14.12.2 Correction of finger posture changes

There are six basic finger posture changes described in Table 14.1.

Type 6 correction: Type 6 finger posture change can be eliminated by rotation around the *z*-axis using rotation matrix $R(\theta)$. To obtain the unknown rotation θ, sets C_{top}, C_{bottom} and $C_{middleline}$ in equation sets below are defined:

$$C_{top} = \{(x,y)|M(x,y) = 1 \wedge M(x,y-1) = 0\}$$
$$C_{bottom} = \{(x,y)|M(x,y) = 1 \wedge M(x,y-1) = 0\}$$
$$C_{middleline} = \{(x,y)|\exists(x,y_T) \in C_{top} \wedge \exists(x,y_B) \in C_{bottom} \wedge yB + yT = 2y\}$$

where $M(x, y)$ is an image segmentation mask. Examples of these sets are visualized in Figure 14.21(b).

Type 3 correction: When the Type 6 posture change is eliminated, it is possible to crop the finger image according to the finger mask to minimize the image size while preserving the ROI. Consequently, the Type 3 change is eliminated as well. This step is visualized in Figure 14.21(d).

Type 1 correction: The Type 1 posture change is trivially solved, since the position of the fingertip is known, and therefore alignment according to left border solves the Type 1 posture change.

Type 5 correction: To eliminate Type 5 posture change, the finger vein image is normalized to a rectangle using a finger image mask. The image with size ($x_{\max}$, $y_{\max}$) is separated by columns and each column segment, where $M(x, y) = 1$ is linearly stretched to the size (1, $y_{\max}$). The result of this operation is displayed in Figure 14.21(e).

Both Types 2 and 4 posture changes are ignored in this work.

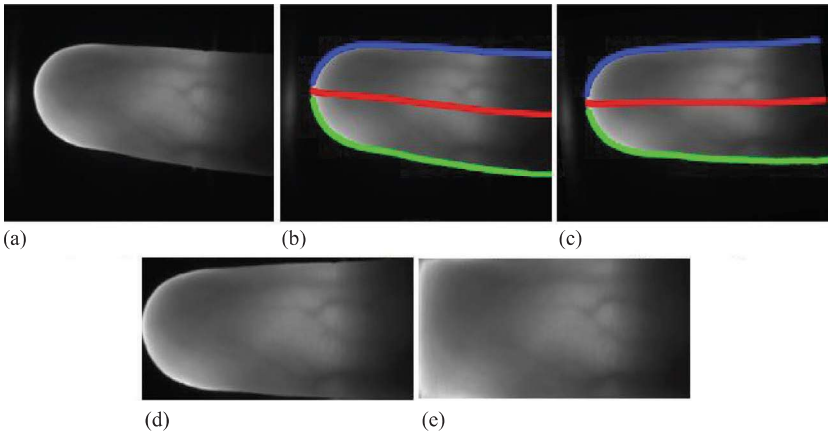

Figure 14.21 Procedure of elimination of finger posture changes—C_{top}, C_{bottom}, $C_{middleline}$ sets: (a) original image, (b) visualized sets C_*, (c) rotated by θ, (d) cropped and (e) stretched

14.12.3 Interphalangeal joint localization

The phalangeal joints of a finger are constituted by several components including synovial fluid [43], the density of which is much lower than the density of bones. Therefore, when using transmission method to acquire a finger vein image, a brighter region can be seen in the acquired image, which corresponds to the interphalangeal joint. This region can be substituted by a single line with a pixel width [43]. The Type 6 change is ignored, and sum of all gray level values for each column (perpendicular to the length of the finger) is computed in (14.3), and the maximum row-sum in (14.4) approximately denotes the position of the interphalangeal joint. After Type 2 correction, it is possible to detect the interphalangeal joint. Better results were obtained using weighted ϕ in (14.5), where smaller weight is given with the length of the finger. This weighting is necessary, due to frequent wrong positioning of the user's finger. The fingertip is then overilluminated and might cause wrongly localized interphalangeal joint.

$$\phi(x) = \sum_{y=1}^{y_{\max}} f(x,y) \tag{14.3}$$

$$r_k = \underset{x\in\{1,\ldots,x_{\max}\}}{\arg\max} \; (\phi(x)) \tag{14.4}$$

$$r_k = \underset{x\in\{1,\ldots,x_{\max}\}}{\arg\max} \left(\sqrt{\frac{x}{x_{\max}}} \cdot \phi(x) \right) \tag{14.5}$$

14.12.4 Size normalization

Having a feature vector of a constant size can be achieved by cropping the stretched image followed by scaling. For cropping, the r_k (interphalangeal joint approximation)

is used as right border and $r_k/8$ is used as a left border. The height of the image is preserved. After that, the cropped image is scaled to size 300×200 pixel.

Due to various thicknesses of fingers of different persons, it is necessary to acquire several images of the same finger with different exposure time. Each finger vein record is contained of a totally ordered set V with six pictures; this set will be denoted as a sequence. There exists a function e: $V \rightarrow N$, which assigns each image an exposure time expressed as a natural number and e is totally ordered on V. The quality estimation function q: $V \rightarrow R$ assigns a score to each image. After that, the image with best score I_{best} is chosen: $I_{best} = \arg\max q(v)$, $(v \in V)$ from the sequence. Several concrete quality estimation approaches can be utilized to choose the best quality image and its score from V and will be presented below.

No heuristic A quality estimation *NoHeuristici*, which statically assigns 1 to the image with the Ith highest exposure time and 0 to others.

Haralick $HaralickF(d, \theta)$ is a quality estimation function, which assigns score to image according to selected Haralick feature F, where $F \in \{Energy, Contrast, Homogenity, Entropy\}$ and displacement vector (d, θ).

An expert can choose a reference image, which histogram will be computed and another image's quality will be estimated by histogram comparison, for example using chi-square method.

14.13 Feature extraction

Various features, which could be extracted from finger vein images, will be described as follows:

- *Local binary patterns* (LBP) is a method for extracting textural features of a grayscale image. The original LBP [44] uses 3*3 nonparametric operator for labeling each pixel (x_c, y_c) by thresholding the eight-neighborhood with the gray level of the center pixel (x_c, y_c) and summing threshold values weighted by powers of two [45].
- *Repeated line tracking:* This method extracts finger vein pattern even from a noised and irregularly shaded image. The method is based on tracking dark lines starting at various pixel positions. The dark line is followed until it is not detectable anymore, and then a new line from different pixel is started.
- *Maximum curvature:* It is claimed to be resistant to various vein widths and its brightness. The algorithm has become a benchmark for the newly developed finger vein extraction and comparison methods [46–48].

The Haralick and Local Binary Patterns Histogram (LBPH) features described were utilized as a texture describing features, which will be mainly used as a discriminative feature for liveness detection.

In the case of Haralick features, all four mentioned (contrast, energy, homogenity and entropy) are concatenated to a single-feature vector. On the other hand,

maximum curvature and repeated line tracking are suited for detailed vein evaluation and therefore finger vein recognition. The outcome of both maximum curvature and repeated line tracking is a locus space with probability of being a vein. This locus space is thresholded using threshold t, computed as t-percentile of nonzero locus space values.

The last step in processing pipeline is dependent on the chosen mode: liveness detection or vein recognition. In the classification mode, binary (with classes live and nonlive) nonlinear probabilistic support vector machine (SVM) with radial basis function (RBF) as a kernel is used for final decision. The recognition mode details are dependent on used feature extraction method. To determine score of two LBPH vectors, a chi-square metric is used. In the case of repeated line tracking and maximum curvature, the veins are aligned using iterative closest point (ICP) algorithm, after that the detected veins are emphasized with morphological operations and the final comparison score is based on Hamming distance of intersecting regions.

14.14 Quality annotator

An application for manual quality annotation of finger vein was implemented for objective evaluation of quality-assessment algorithms. It scans for all sets of six images from the same session and then it displays them on screen using QT framework7. An expert can then assign the images a label (good or bad) as can be seen in Figure 14.22. The output of quality annotator can be used in evaluation subsystem to evaluate different approaches of quality assessment.

14.15 Dataset description

To evaluate the proposed system, a dataset containing both live fingers and fingers spoofs was gathered. Six fingers (both index, middle and ring fingers) of each volunteer were captured, and each finger can be perceived as a biometric sample of a unique individual. Each finger was captured six times in two different days to consider possible changes of vein visibility. The nonlive dataset consists of 370 sequences of 59 different materials or material combinations.

14.16 Conclusion

In this chapter, we have introduced multiple general approaches that can and are being used for purposes of liveness detection in hand and finger-based biometrics. Methods based on spectral analysis have been further elaborated on. The principle using the light absorption as well as light reflection has been discussed, and a method of acquiring data described. The advantages, disadvantages and results of mentioned approaches to liveness detection were discussed.

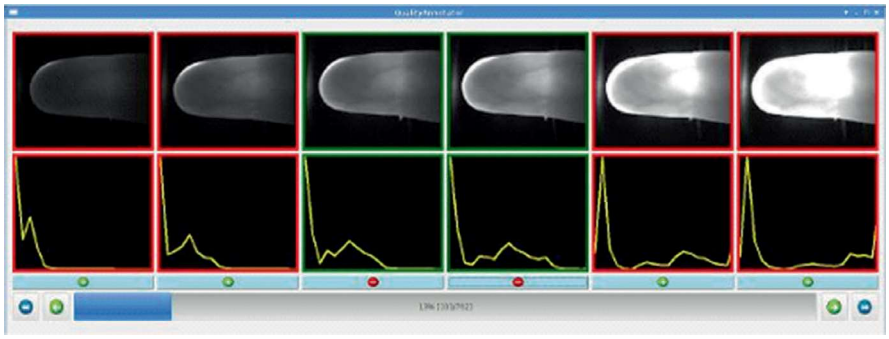

Figure 14.22 Screenshot of quality annotator application. The images highlighted with green color was marked as good; on the other hand, images highlighted with red are marked as poor quality images

Lately, the spoofing attacks have shown that it is possible to fool most commercial fingerprint sensors with artificial fingerprints. On the contrary, finger vein recognition is a relatively new but promising method suitable for biometric authentication achieving high recognition performance. One advantage of vein recognition is that blood vessels are an internal biometric characteristic, and it is harder for an attacker to obtain it from a user. Image of veins is usually acquired using infrared radiation for biometric purposes. When we create a biometric system, which examines both mentioned characteristics at once, it is more demanding to compromise it. An intruder must obtain both fingerprint and image of finger veins of a legitimate user and merge those into a single spoof, which has desired optical characteristics. All implemented methods were thoroughly evaluated and compared. In liveness detection mode, EER equal to 6.5% was achieved using LBPH features. In finger vein verification mode, the best result EER equal to 10.8% was obtained using maximum curvature features. A future development, which may improve the error rates, was outlined including reconstruction of 3D model of blood vessels. As we can see, the error rates are quite high for unimodal system, but in fusion with high precision fingerprint recognition, it might be possible to preclude most of impostor attempts without rejecting any legitimate user.

Acknowledgment

This work was supported by The Ministry of Education, Youth and Sports of the Czech Republic from the National Programme of Sustainability (NPU II); project IT4Innovations excellence in science—LQ1602.

References

[1] Jain, A.K., Flynn, P. and Ross, A.A. *Handbook of Biometrics.* Springer-Verlag New York, Inc., Secaucus, NJ, USA, 2007. ISBN: 978-0387710402.

[2] Sandstrfom, M. *Liveness Detection in Fingerprint Recognition Systems*. Ph.D. thesis, Linköping University, 2004. Available at: http://www.diva-portal.org/smash/get/diva2:19729/FULLTEXT01.pdf.

[3] Feng, J., Jain, A.K. and Ross, A. *Fingerprint Alteration.* Tech. Rep. MSU-CSE-09-30, Department of Computer Science, Michigan State University, East Lansing, Michigan, Dec. 2009.

[4] Drahanský, M. *Liveness Detection in Biometrics*. InTech—Open Access Publisher, Rijeka, 2011, pp. 179–198. ISBN: 978-953-307-487-0.

[5] Drahanský, M., Funk, W. and Nötzel, R. *Liveness Detection based on Fine Movements of the Fingertip Surface*. In: IEEE – The West Point Workshop, West Point, New York, 2006, pp. 42–47. ISBN: 1-4244-0130-5.

[6] Drahanský, M. *Methods for Quality Determination of Papillary Lines in Fingerprints*. NIST, Gaithersburg, 2007, p. 25.

[7] Drahanský, M. and Lodrová, D. *Liveness Detection for Biometric Systems Based on Papillary Lines*. In: 2008 International Conference on Information Security and Assurance (ISA 2008) [online]. IEEE, 2008, pp. 439–444 [cit. 2017-10-13]. DOI: 10.1109/ISA.2008.58. ISBN: 978-0-7695-3126-7.

[8] Shahzad, A. M. *Novel Active Sweat Pores Based Liveness Detection Techniques for Fingerprint Biometrics*. Brunel University, 2012. Available at: http://bura.brunel.ac.uk/bitstream/2438/7060/1/FulltextThesis.pdf.

[9] Shuckers, S., Hornak, L., Norman, T., Derakhshani, R. and Parthnasardi, S. *Issues for Liveness Detection in Biometrics*. West Virginia University, 2006. Available at: http://www.biometrics.org/bc2002/2bc0130 DerakhshabiBrief.pdf.

[10] Drahanský, M. *Liveness Detection in Biometrics*. Chetty, Girija, ed. Advanced Biometric Technologies [online]. InTech, 2011 [cit. 2017-11-12]. DOI: 10.5772/17205. ISBN: 978-953-307-487-0.

[11] Hartung, D. *Vascular Pattern Recognition and its Application in Privacy-Preserving Biometric Online-Banking Systems*. Ph.D. thesis, Gjøvik University College, 2012. ISBN: 978-82-93269-01-4.

[12] Fuksis, R., Greitans, M., Nikisins, O. and Pudzs, M. *Infrared imaging system for analysis of blood vessel structure*. Elektronika ir Elektrotechnika 97, 1 (2010), pp. 45–48. ISSN: 2029-5731.

[13] Anderson, R.R. and Parrish, J.A. *The optics of human skin*. Journal of Investigative Dermatology 77, 1 (1981), pp. 13–19. ISSN: 0022-202X.

[14] Hashimoto, J. *Finger vein authentication technology and its future*. In: VLSI Circuits, 2006. Digest of Technical Papers. 2006 Symposium on (2006), pp. 5–8. ISBN: 1-4244-0006-6.

[15] Yang, J. and Shi, Y. *Towards finger-vein image restoration and enhancement for finger-vein recognition*. Information Sciences 268 (2014), pp. 33–52. ISSN: 0020-0255.

[16] Drahanský, M., Orság, F. and Doležel, M. *Biometrie*, 2011, p. 294. ISBN: 978-80-254-89796.

[17] Drahanský, M., Dvořák, R., Váňa, J., Goldmann, T., Dvořák, M. and Kanich, O. *A multispectral lifecycle detector especially suited for the fingerprint recognition technology*. Utility model no. 31405, Touchless Biometric Systems, 2018.

[18] Leoš, N. *Nové pohledy na neinvazivní laser (New views of non-invasive laser)*. Grada Publishing, 2015. ISBN: 978-80-247-1651-0.

[19] Drahanský, M., Doležel, M., Váňa, J., Březinová, E., Yim, J. and Shim, K. *New optical methods for liveness detection on fingers*. BioMed Research International [online]. 2013 (2013), pp. 1–11 [cit. 2017-10-13]. DOI: 10.1155/2013/197925. ISSN 2314-6133.

[20] Drahanský, M. *Liveness Detection on Fingers*. Advanced Biometric Technologies. InTech—Open Access Publisher, 2011. ISBN: 978-953-307-487-0. Available at: https://www.intechopen.com/books/advanced-biometric-technologies/liveness-detection-in-biometrics.

[21] Touchless Biometric Systems. 3D Enroll—touchless fingerprinting—datasheet [online]. Available at: https://www.tbs-biometrics.com/files/documents/en/TBS_Productsheet_E_3D-ENROLL-07-2017.pdf [Accessed 13 Oct. 2017].

[22] Brown, R. and Davenport J. *Forensic Science: Advanced Investigations*. South-Western Educational Pub, 2011. ISBN: 978-0538450898.

[23] Gleason, C.A. and Juul, S.E. *Avery's Diseases of the Newborn*. E-Book. Elsevier Health Sciences, 2011. ISBN: 9780323401395.

[24] Pryse-Phillips, W. *Companion to Clinical Neurology*. Oxford University Press, 2009. ISBN: 978-0195367720.

[25] Leybell, I. *Auricular Hematoma Drainage* [online]. Available at: https://emedicine.medscape.com/article/82793-overview [Accessed 9 Nov. 2017].

[26] Hardt, N. and Kuttenberger, J. *Craniofacial Trauma: Diagnosis and Management*. Springer Science & Business Media, 2010, ISBN: 978-3-540-33041-7.

[27] Reich, D., Psomadakis, C.E. and Buka, B. *Subungual Hematoma*. In: Top 50 Dermatology Case Studies for Primary Care. Springer, 2017, pp. 125–130, ISBN: 978-3-319-18626-9.

[28] Davis, C.P. *Hemoglobin (Low and High Range Causes)* [online]. Available at: https://www.medicinenet.com/hemoglobin/article.htm [Accessed 9 Nov. 2017].

[29] Thunderpath Media Inc. (2013). *The Stages of Contusion* [online]. Available at: http://www.baronerocks.com/index.php/mnemonics/467-the-stages-of-a-contusion [Accessed 8 Nov. 2017].

[30] Vanezis, P. *Interpreting bruises at necropsy*. Journal of Clinical Pathology 54, 5 (2001), pp. 348–355.

[31] Lecomte, M.J., Holmes, T., Kay, D.P., Simons, J.L. and Vintiner, S.K. *The use of photographs to record variation in bruising response in humans*. Forensic Science International 231, 1 (2013), pp. 213–218.

[32] Clark, V.L. and Kruse, J.A. *Clinical methods: the history, physical, and laboratory examinations*. The Journal of the American Medical Association 264, 21 (1990), pp. 2808–2809.

[33] McGee, S. *Evidence-Based Physical Diagnosis*. E-Book. Elsevier Health Sciences, 2016. ISBN: 978-0323392761.

[34] Kaneko, J.J., Harvey, J.W. and Bruss, M.L. (ed.). *Clinical Biochemistry of Domestic Animals*. Academic Press, 2008. ISBN: 978-0123704917.

[35] Stave, U. (ed.). *Perinatal Physiology*. Springer Science & Business Media, 2013. ISBN: 9781468423167.

[36] Damjanov, I. *Pathology Secrets*. Elsevier Health Sciences, 2009. ISBN: 978-0323055949.

[37] Huang, Z.K. and Liu, D.H. *Segmentation of Color Image Using EM Algorithm in HSV Color Space*. In: 2007 International Conference on Information Acquisition, Seogwipo-si, 2007, pp. 316–319. DOI: 10.1109/ICIA.2007.4295749.

[38] Solomon, C. and Breckon, T. *Fundamentals of Digital Image Processing: A Practical Approach with Examples in Matlab*. John Wiley & Sons, 2011. ISBN: 978-0470844731.

[39] Donaldson, A.E. and Lamont, I.L. *Biochemistry changes that occur after death: potential markers for determining post-mortem interval*. PLoS ONE 8, 11 (2013), p. e82011.

[40] Huang, B., Dai, Y., Li, R., Tang, D. and Li, W. *Finger-vein authentication based on wide line detector and pattern normalization*. In Pattern Recognition (ICPR), 2010 20th International Conference on (2010), IEEE, pp. 1269–1272. ISBN: 978-1-4244-7542-1.

[41] Miura, N., Nagasaka, A. and Miyatake, T. *Feature extraction of finger-vein patterns based on repeated line tracking and its application to personal identification*. Machine Vision and Applications 15, 4 (Oct. 2004), pp. 194–203. ISSN: 0932-8092.

[42] Huang, B., Liu, S. and Li, W. *A finger posture change correction method for finger-vein recognition*. In: Computational Intelligence for Security and Defence Applications (CISDA), 2012 IEEE Symposium on (Jul. 2012), pp. 1–7. ISBN: 978-1-4673-1416-9.

[43] Yang, J. and Shi, Y. *Finger-vein ROI localization and vein ridge enhancement*. Pattern Recognition Letters 33, 12 (2012), pp. 1569–1579. ISSN: 0167-8655.

[44] Park, K.R. *Finger vein recognition by combining global and local features based on SVM*. Computing and Informatics 30, 2 (2011), pp. 295–309. ISSN: 1335-9150.

[45] Ahonen, T., Matas, J., He, C. and Pietikäinen, M. *Rotation invariant image description with local binary pattern histogram Fourier features*. In: Proceedings of the 16th Scandinavian Conference on Image Analysis (Berlin, Heidelberg, 2009), SCIA '09, Springer-Verlag, pp. 61–70. ISBN: 978-3-642-02229-6.

[46] Zhang, H., Liu, Z., Zhao, Q., Zhang, C. and Fan, D. *Finger vein recognition based on Gabor filter*. In: Intelligence Science and Big Data Engineering, C. Sun, F. Fang, Z.-H. Zhou, W. Yang, and Z.-Y. Liu, Eds., Vol. 8261 of Lecture Notes in Computer Science. Springer Berlin Heidelberg, 2013, pp. 827–834. ISBN: 978-3-642-42056-6.

[47] Raghavendra, R., Raja, K., Surbiryala, J. and Busch, C. *A low-cost multi-modal biometric sensor to capture finger vein and fingerprint*. In: Biometrics (IJCB), 2014 IEEE International Joint Conference on (Sep. 2014), pp. 1–7. ISBN: 978-1-4799-3585-7.

[48] Ton, B.T. and Veldhuis, R.N. *A high quality finger vascular pattern dataset collected using a custom designed capturing device.* In: Biometrics (ICB), 2013 International Conference on (2013), IEEE, pp. 1–5. ISBN: 978-1-4799-0310-8.